

Supporting Information

**Multilayered Ceramic Membrane with Ion Conducting Thin Layer  
Induced by Interface Reaction for Stable Hydrogen Production**

*G. He, Q. Lan, M. Liu, G. Wu, R. E. Dunin-Borkowski, H. Jiang\**

# Supporting Information

**This file includes:**

Supplementary Information  
Figs. S1 to S26  
Table S1

## Experimental materials and methods

### 1. Preparation of multilayered ceramic membranes with CeO<sub>2</sub> or YSZ thin layers

All eleven dual-phase composite primary powders:

- Ce<sub>0.9</sub>Gd<sub>0.1</sub>O<sub>2-δ</sub>-Gd<sub>0.1</sub>Sr<sub>0.9</sub>Fe<sub>0.9</sub>Ti<sub>0.1</sub>O<sub>3-δ</sub> (CGO-GSFT) (CGO/GSFT ratio = 7/3, 6/4, 3/7)
- Ce<sub>0.9</sub>Gd<sub>0.1</sub>O<sub>2-δ</sub>-Gd<sub>0.1</sub>Sr<sub>0.9</sub>FeO<sub>3-δ</sub> (CGO-GSF)
- Ce<sub>0.9</sub>Gd<sub>0.1</sub>O<sub>2-δ</sub>-La<sub>0.2</sub>Sr<sub>0.8</sub>Fe<sub>0.8</sub>Co<sub>0.2</sub>O<sub>3-δ</sub> (CGO-LSFC)
- Ce<sub>0.9</sub>Gd<sub>0.1</sub>O<sub>2-δ</sub>-SrFe<sub>0.8</sub>Co<sub>0.2</sub>O<sub>3-δ</sub> (CGO-SFC)
- Ce<sub>0.9</sub>Gd<sub>0.1</sub>O<sub>2-δ</sub>-SrFe<sub>0.5</sub>Ce<sub>0.5</sub>O<sub>3-δ</sub> (CGO-SFCe)
- Ce<sub>0.9</sub>Pr<sub>0.1</sub>O<sub>2-δ</sub>-Pr<sub>0.6</sub>Sr<sub>0.4</sub>FeO<sub>3-δ</sub> (CPO-PSF)
- Ce<sub>0.9</sub>Pr<sub>0.1</sub>O<sub>2-δ</sub>-Pr<sub>0.6</sub>Sr<sub>0.4</sub>Fe<sub>0.8</sub>Co<sub>0.2</sub>O<sub>3-δ</sub> (CPO-PSFC)
- Ce<sub>0.9</sub>Sm<sub>0.1</sub>O<sub>2-δ</sub>-Sm<sub>0.1</sub>Sr<sub>0.9</sub>FeO<sub>3-δ</sub> (SDC-SSF)
- Ce<sub>0.9</sub>Sm<sub>0.1</sub>O<sub>2-δ</sub>-La<sub>0.1</sub>Sr<sub>0.9</sub>FeO<sub>3-δ</sub> (SDC-LSF)
- Ce<sub>0.9</sub>Gd<sub>0.1</sub>O<sub>2-δ</sub>-NiFe<sub>2</sub>O<sub>4</sub> (CGO-NFO)
- Y<sub>0.08</sub>Zr<sub>0.92</sub>O<sub>2-δ</sub>-CoFe<sub>2</sub>O<sub>4</sub> (YSZ-CFO)

were synthesized using a combined citric acid and ethylenediaminetetraacetic acid (EDTA) method, which is described in detailed elsewhere [1].

During the typical preparation process of a three-layered ceramic membrane, 0.6 g of as-prepared CGO-GSFT powder, 0.16 g of corn starch and 0.04 g of carbon fiber were well mixed in a mortar. After drying, the resultant powder was uniaxially pressed into a disk. 120 mg of as-prepared CGO-GSFT powder without pore former was then homogeneously spread onto the above pre-pressed disk and co-pressed at 20 MPa for 5 mins. The resulting green disk was sintered at 1450 °C on a corundum substrate in air for 10 hours. Finally, a three-layered ceramic membrane was obtained with a ~3-μm-thick CGO dense layer adjacent to a ~100-μm-thick functional layer and a ~700-μm-thick porous support layer.

During the typical preparation process of a bilayer ceramic membrane, for example, (0.6 - 1.0) g of as-prepared CGO-GSFT powder was uniaxially pressed into a disk at 20 MPa for 5 mins. The resulting green disk was sintered at 1350 ~ 1500 °C on a corundum substrate in air for a few hours. Finally, a bilayer ceramic membrane was obtained with a CGO dense thin layer adjacent to a CGO-GSFT parent layer.

For the preparation process of a CGO-GSFT-Al<sub>2</sub>O<sub>3</sub> composite system, as-prepared CGO-GSFT powder and commercial Al<sub>2</sub>O<sub>3</sub> powder (fired at 1300 °C for 10h) were well mixed in a mortar. Some of the resultant powder was measured by using high-temperature X-ray diffraction. Some of the resultant powder was uniaxially pressed at 20 MPa for 5 mins into a disk. The resulting green disk was sintered at 1450 °C on a corundum substrate in air for 10 hours.

### 2. Characterization

Phase formation was investigated using X-ray diffraction (Cu K $\alpha$ , Bruker D4).

Scanning electron microscopy, back scattered microscopy and energy dispersive X-ray spectroscopy (Prisma E, Thermo Fisher Scientific) integrated with a pathfinder X-ray microanalysis system were employed to investigate surface/cross-sectional morphologies and elemental distributions of all layered ceramic membranes with Ce<sub>0.9</sub>Mo<sub>0.1</sub>O<sub>2- $\delta$</sub>  thin layers, the used corundum substrate, specimens before and after CO<sub>2</sub> or wet H<sub>2</sub> treatment, and the bi-layered CGO/(CGO-GSFT) specimens before and after membrane tests. Cross-sectional back scattered electron (BSE) images of the layered ceramic membranes with CSO, CPO, YSZ and CGO thin layers shown in Fig. 2f were obtained in an SEM after ion milling (IM4000PLUS, HITACHI Co., Ltd, Japan) using an Ar ion beam.

Cross-sectional samples containing CGO dense layers were prepared using focused ion beam (FIB) milling in an FEI Helios Nanolab 400s dual beam system. The samples were further polished using a 500 eV Ar ion beam (Fischione Nanomill, model 1040) to remove surface damaged layers introduced by FIB milling. High-angle annular dark-field (HAADF) scanning transmission electron microscopy (STEM) and energy-dispersive X-ray spectroscopy (EDX) mapping were performed in an FEI Titan G2 80-200 ChemiSTEM microscope equipped with a high-brightness field emission gun, a probe Cs corrector and a super-X EDX system.

Simultaneous thermogravimetric analysis (TGA) and differential scanning calorimetry (DSC) analyses were performed on a NETZSCH STA 449F5 system under flowing synthetic air. A high temperature XRD measurement of CGO-GSFT-Al<sub>2</sub>O<sub>3</sub> was performed using Cu K $\alpha$  radiation in a Rigaku SmartLab9kw diffractometer equipped with a RT1500 high temperature chamber at a 10 °C min<sup>-1</sup> heating rate in an ambient atmosphere between 25 and 1500 °C. The acquisition time for each diffractogram was approximately 30 mins.

Adhesion between the CGO thin-layer and the CGO-GSFT parent layer was evaluated using scratch tests (MFT-4000, Lanzhou Huahui Instrument Technology, China). The tests was performed by increasing the normal load from 0 to 50 N on a predetermined scratch length of 5 mm at a loading rate of 30 N/min. Determination of the critical loads was assisted by measuring the acoustic emission and friction force during scratching, as well as by using a BSE measurement to visually identify the scratch tracks.

Atomic-force microscopy (AFM, Agilent 5400) was employed to examine the surface microstructures of the CGO thin layer and the used Al<sub>2</sub>O<sub>3</sub> substrate.

### 3. Membrane performance tests

A bi-layered CGO/(CGO-GSFT) membrane pellet was sealed onto an alumina tube using a silver ring and kept in the middle of an oven under isothermal conditions. The effective membrane area was 0.78 cm<sup>2</sup>. The membrane separator configuration is described elsewhere [2]. A Ni-based catalyst (0.3 g, Süd Chemie AG) was loaded on the dense CGO-enriched layer of the CGO/(CGO-GSFT) layered membrane. As reported in previous work [3], the membrane leakage caused by imperfect sealing was checked by measuring the nitrogen content in the permeated gas according to the feed synthetic air and the sweep helium. Afterwards, two sides of the membrane were successively exposed to six different conditions (air/He, air/CO<sub>2</sub>, air/CH<sub>4</sub>, Ar-H<sub>2</sub>O/CH<sub>4</sub>, He-H<sub>2</sub>O/H<sub>2</sub>-CH<sub>4</sub>-CO<sub>2</sub>-N<sub>2</sub>, He-H<sub>2</sub>O/H<sub>2</sub>-CH<sub>4</sub>-CO<sub>2</sub>-N<sub>2</sub>-H<sub>2</sub>S) at 925 °C for oxygen permeation flux measurements. The flow rates of the gases at the feed and sweep sides of the membrane were as follows:

- ① F(air) = 30 cm<sup>3</sup> min<sup>-1</sup>; F(He) = 20 cm<sup>3</sup> min<sup>-1</sup>
- ② F(air) = 20 cm<sup>3</sup> min<sup>-1</sup>; F(CO<sub>2</sub>) = 10 cm<sup>3</sup> min<sup>-1</sup>
- ③ F(air) = 20 cm<sup>3</sup> min<sup>-1</sup>; F(CH<sub>4</sub>) = 6 cm<sup>3</sup> min<sup>-1</sup>
- ④ F(H<sub>2</sub>O) = 16 cm<sup>3</sup> min<sup>-1</sup>, F(Ar) = 4 cm<sup>3</sup> min<sup>-1</sup>, F(CH<sub>4</sub>) = 6 cm<sup>3</sup> min<sup>-1</sup>
- ⑤ F(H<sub>2</sub>O) = 16 cm<sup>3</sup> min<sup>-1</sup>, F(He) = 4 cm<sup>3</sup> min<sup>-1</sup>; F(H<sub>2</sub>) = 6 cm<sup>3</sup> min<sup>-1</sup>, F(CH<sub>4</sub>) = 4 cm<sup>3</sup> min<sup>-1</sup>, F(CO<sub>2</sub>) = 1 cm<sup>3</sup> min<sup>-1</sup>, F(N<sub>2</sub>) = 2 cm<sup>3</sup> min<sup>-1</sup>
- ⑥ F(H<sub>2</sub>O) = 16 cm<sup>3</sup> min<sup>-1</sup>, F(He) = 4 cm<sup>3</sup> min<sup>-1</sup>; F(H<sub>2</sub>) = 6 cm<sup>3</sup> min<sup>-1</sup>, F(CH<sub>4</sub>) = 4 cm<sup>3</sup> min<sup>-1</sup>, F(CO<sub>2</sub>) = 1 cm<sup>3</sup> min<sup>-1</sup>, F(N<sub>2</sub>) = 2 cm<sup>3</sup> min<sup>-1</sup>, H<sub>2</sub>S concentration = 37 ppm.

The flow rates of the gas were controlled by gas mass flow controllers (Bronkhorst). The H<sub>2</sub>O flow was controlled by a liquid mass flow controller (Bronkhorst) and evaporated at 160 °C before it was fed to the reactor. The lines from the outlets to the gas chromatograph were heated to 160 °C. The gas composition was analyzed using an online gas chromatograph (GC, Agilent 7890B). The oxygen permeation fluxes were calculated from the amount of oxygen in the inlet and outlet streams on the air side or from the amount of generated hydrogen in the outlet streams on the H<sub>2</sub>O side [4].

A catalytic membrane with a sandwich-like asymmetric configuration for COG-oxidation driven water splitting was obtained using one single sintering and slurry coating process. A three-layered ceramic membrane, consisting of a porous CGO-GSFT backbone, a CGO-GSFT intermediate layer and a dense CGO thin-layer, was prepared after one single sintering at 1450 °C for 10 hours. Afterwards, CGO slurry was deposited directly on the layered ceramic membrane by drop-coating. The membrane was dried and annealed at 1200 °C for 2 hours in air. The thickness of the porous CGO layer was ~10 μm. Catalyst particles in the backbone and CGO porous layer were produced by wet impregnation with a solution containing 0.02 mol L<sup>-1</sup> ruthenium nitrosyl nitrate, followed by firing in air at 800 °C for 1 hour to convert the ruthenium nitrosyl nitrate into ruthenium oxide. After several cycles of infiltration, ~5 wt.% RuO<sub>2</sub> loading was achieved in the multilayered catalytic

membrane.

- ❖ For the investigation of H<sub>2</sub> production rates from water splitting as a function of H<sub>2</sub>/(CH<sub>4</sub>+H<sub>2</sub>) ratio in simulated COG stream, the operating conditions were as follows: temperature: 925 °C, H<sub>2</sub>O side: H<sub>2</sub>O/He = 20 / 5 cm<sup>3</sup> min<sup>-1</sup>; simulated COG side: F(total) = 6 cm<sup>3</sup> min<sup>-1</sup> including 3 cm<sup>3</sup> min<sup>-1</sup> N<sub>2</sub>, and H<sub>2</sub> concentration of 0, 16.67, 33.33, 41.67 and 50 vol.%.
- ❖ Effect of H<sub>2</sub>S concentration in a simulated COG stream on hydrogen production rates from water splitting. H<sub>2</sub>O side: 20 cm<sup>3</sup> min<sup>-1</sup> H<sub>2</sub>O + 5 cm<sup>3</sup> min<sup>-1</sup> He; simulated COG side: 2 cm<sup>3</sup> min<sup>-1</sup> H<sub>2</sub> + 1 cm<sup>3</sup> min<sup>-1</sup> CH<sub>4</sub> + ppm level H<sub>2</sub>S, Temperature: 925 °C.

#### 4. Computational thermodynamics calculations

In order to understand the possible interfacial solid-state reactions, thermodynamic calculations were performed with FactSage8.1 [5] using the FToxid, FactPS and AIMP [6] databases. When a compound is available, the database used follows the priority: FToxid > FactPS > AIMP. The change in Gibbs energy and enthalpy of the eight possible reactions proposed (see Fig. S1) was calculated. The equilibrium calculation at the interface or local reaction zones around the interface was not considered in this work due to a lack of diffusion data.

#### 5. Calculation of the enthalpy change of SrO + Al<sub>2</sub>O<sub>3</sub> → SrAl<sub>2</sub>O<sub>4</sub> reaction

In order to calculate the standard enthalpy of solid-state reaction between SrO and Al<sub>2</sub>O<sub>3</sub> producing SrAl<sub>2</sub>O<sub>4</sub> (SrO + Al<sub>2</sub>O<sub>3</sub> → SrAl<sub>2</sub>O<sub>4</sub>), we need to look up the standard enthalpies of formation for SrO, Al<sub>2</sub>O<sub>3</sub> and SrAl<sub>2</sub>O<sub>4</sub>, respectively. These data are typically found from previous studies as following [7]:

$$\begin{aligned}\Delta H_f^\ominus \text{ SrO (s, 298K)} &\approx -590.3 \text{ kJ mol}^{-1}, \\ \Delta H_f^\ominus \alpha\text{-Al}_2\text{O}_3 \text{ (s, 298K)} &\approx -1675.7 \text{ kJ mol}^{-1}, \\ \Delta H_f^\ominus \text{ SrAl}_2\text{O}_4 \text{ (s, 298K)} &\approx -2338.9 \text{ kJ mol}^{-1}.\end{aligned}$$

Therefore, the standard enthalpy change ( $\Delta H_r^\ominus$ ) for SrO + Al<sub>2</sub>O<sub>3</sub> → SrAl<sub>2</sub>O<sub>4</sub> can be calculated according to

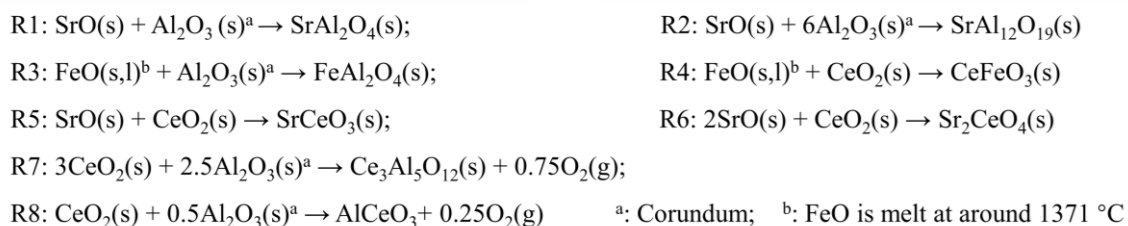
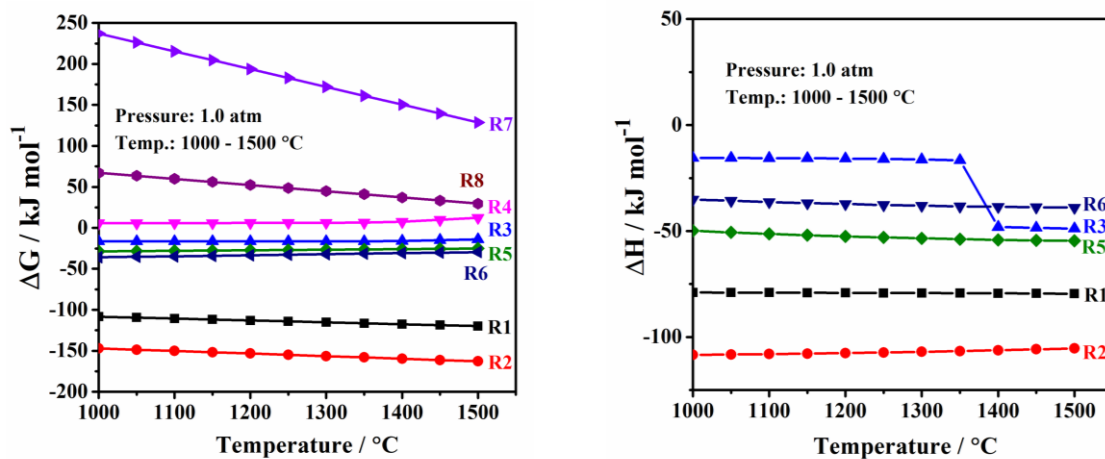
$$\Delta H_r^\ominus = \sum \Delta H_f^\ominus(\text{products}) - \sum \Delta H_f^\ominus(\text{reactants}) = -72.9 \text{ kJ mol}^{-1}$$

In combination with the fact that the heat capacity of SrAl<sub>2</sub>O<sub>4</sub> is larger than that of SrO and Al<sub>2</sub>O<sub>3</sub> from room temperature to 1000 °C [7], the enthalpy change of the solid-state reaction (SrO + Al<sub>2</sub>O<sub>3</sub> → SrAl<sub>2</sub>O<sub>4</sub>) at 1000 °C should be negative, indicating that the reaction at 1000 °C is exothermic, consistent with the calculation results in Fig. S1.

#### 6. The chemical stability and mixed conductivity of ceria-based membranes

In comparison to Pd-based membranes [8], fossil-derived hydrogen-assisted water splitting using a dense mixed ionic-electronic conducting (MIEC) ceramic membrane has been recognized as a promising H<sub>2</sub>-purification technique with respect to low cost and 100% oxygen permeation selectivity. Among MIEC

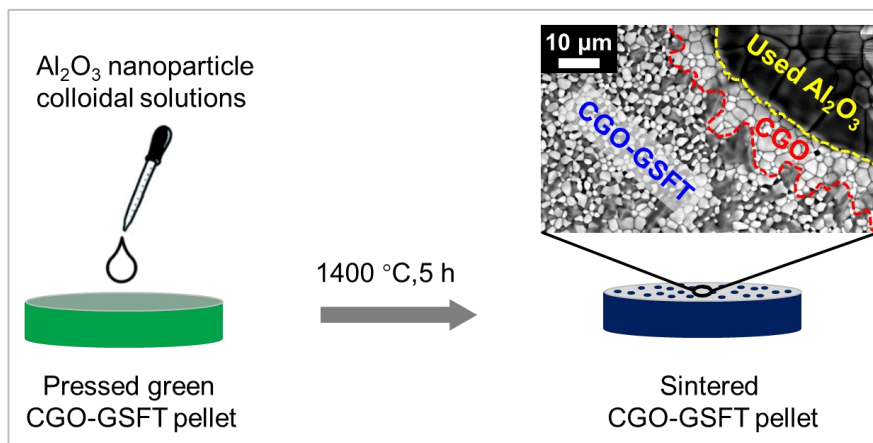
membranes, both Co- and Fe-free membranes, such as  $\text{Ce}_{0.9}\text{Gd}_{0.1}\text{O}_{2-\delta}$ <sup>[9]</sup>,  $\text{Pr}_x\text{Ce}_{0.9-x}\text{Gd}_{0.1}\text{O}_{1.95-x}$ <sup>[10]</sup> and  $\text{Ce}_{0.9}\text{Pr}_{0.1}\text{O}_{2-\delta}-\text{Pr}_{0.1}\text{Sr}_{0.9}\text{Ti}_{0.9}\text{Mg}_{0.1}\text{O}_{3-\delta}$ <sup>[11]</sup>, exhibited high tolerances to  $\text{CO}_2$  and reducing environment, but the hydrogen production rates using these stable MIEC membranes are generally low ( $< 0.3 \text{ cm}^3 \text{ min}^{-1} \text{ cm}^{-2}$ ), owing to their low oxygen permeation fluxes.



**Figure S1.**

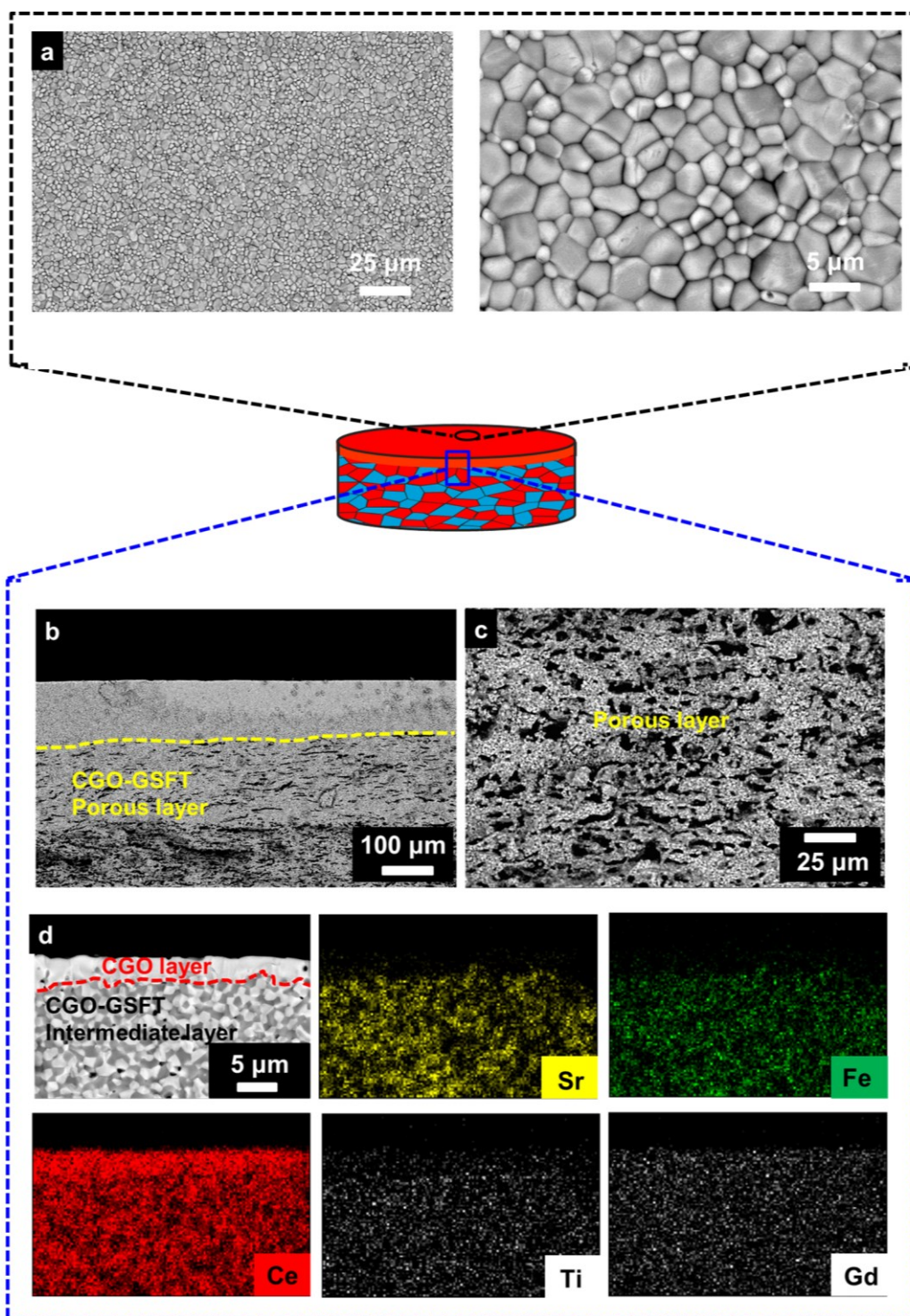
Gibbs free energy and enthalpy change of possible reactions of the SrO-FeO-CeO<sub>2</sub>-Al<sub>2</sub>O<sub>3</sub> system between 1000 and 1500 °C.

As shown in Fig. S1, among the eight possible reactions the changes in Gibbs free energy of R1-R3 and R5-R6 are negative, so these reactions proceed spontaneously and are referred to as exergonic (*i.e.*, exothermic reactions). In particular, the formation of strontium aluminates (SrAl<sub>2</sub>O<sub>4</sub> and SrAl<sub>12</sub>O<sub>19</sub>) proceeds even more energetically downhill, indicating that there is a thermodynamic preference for strontium aluminate products when the composite oxides are exposed to ambient atmosphere between 1000 and 1500 °C.



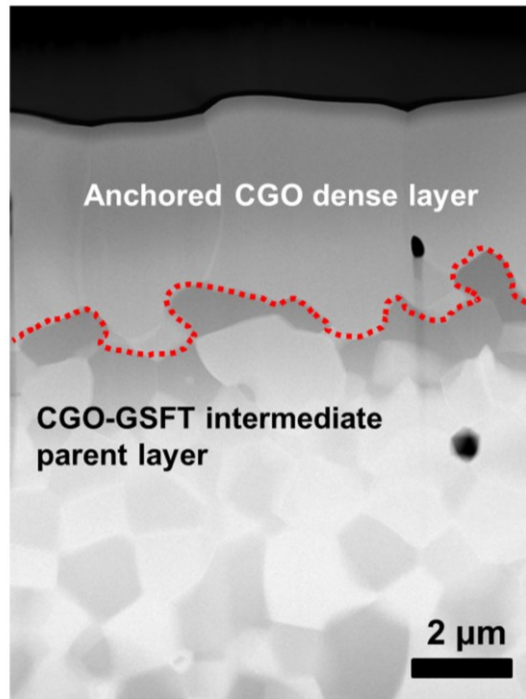
**Figure S2.**

The surface rearrangement of CGO-GSFT membrane coated with  $\text{Al}_2\text{O}_3$  nanoparticles after a sintering process. It was found that a CGO compact layer was formed around the  $\text{Al}_2\text{O}_3$  particle.



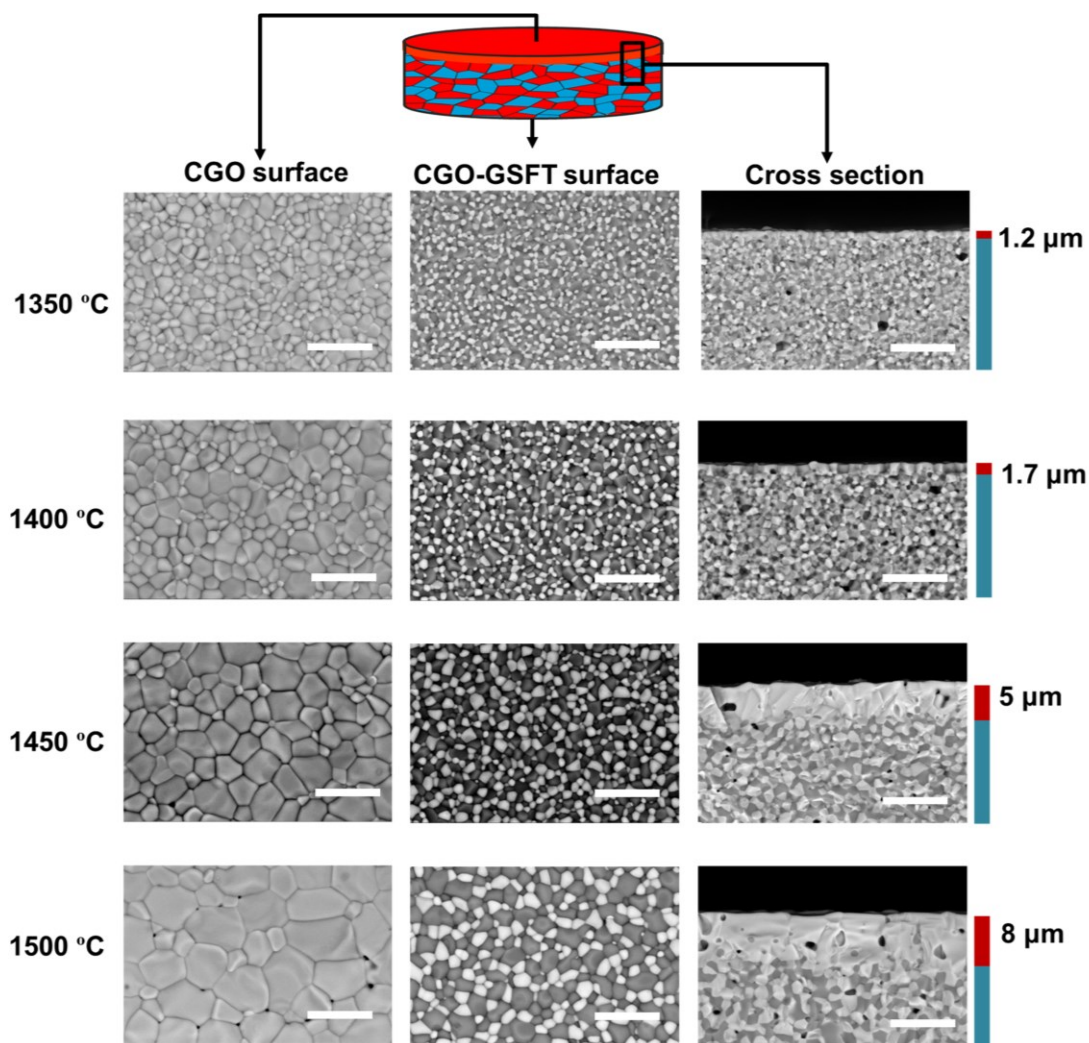
**Figure S3.**

BSE-EDX analyses of (a) the CGO layer and (b-d) the cross section of a CGO/(CGO-GSFT)/porous (CGO-GSFT) three-layered ceramic membrane after a single sintering process.



**Figure S4.**

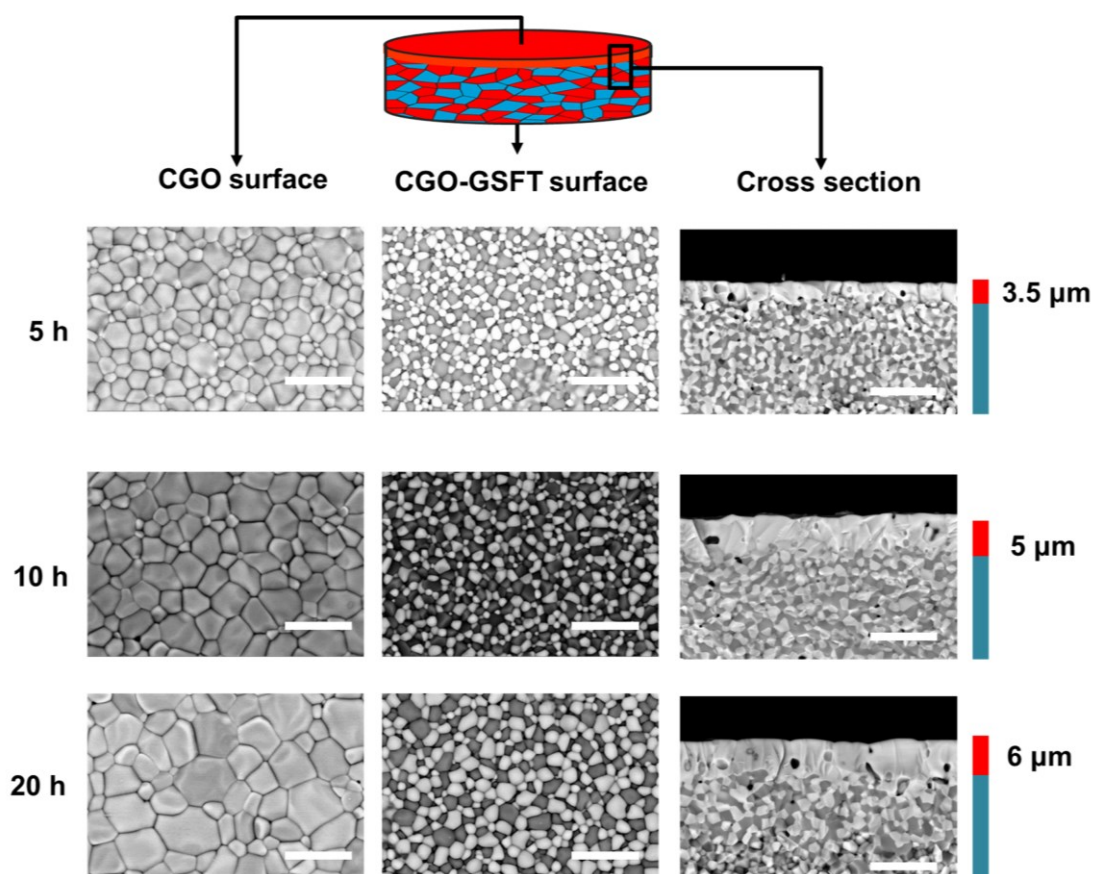
HAADF STEM image of a cross-sectional sample of a CGO/(CGO-GSFT) bi-layered membrane, showing that the CGO thin layer is well riveted into the CGO-GSFT parent layer, indicating good adhesion between the CGO and CGO-GSFT layers.



**Figure S5.**

BSE analyses of the lower surface, top surface and cross-section of 60 mol.% CGO - 40 mol.% GSFT green pellets sintered on  $\text{Al}_2\text{O}_3$  substrates at 1350, 1400, 1450 and 1500 °C for 10 hours in ambient air. The scale bar is 10  $\mu\text{m}$ .

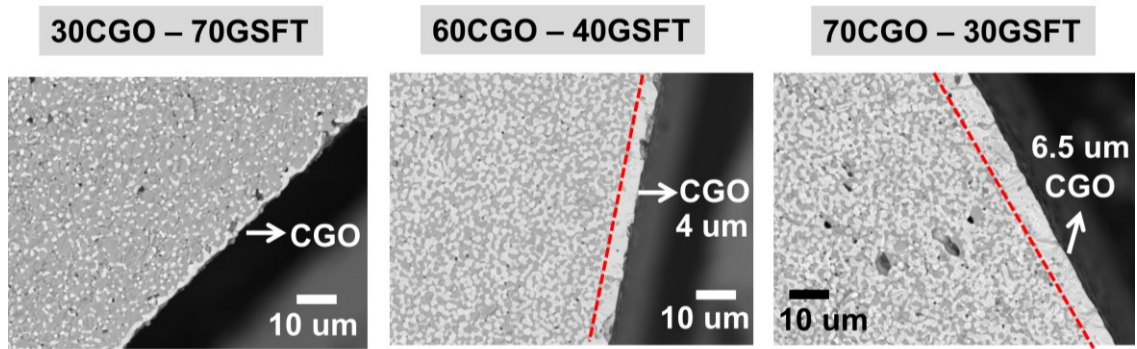
As shown in Fig. S5, the thickness of the CGO layer increases with increasing sintering temperature from 1350 to 1500 °C, indicating that interface-reaction-induced CGO rearrangement and sintering is thermally favorable.



**Figure S6.**

BSE analysis of the surface and cross-section of 60 mol.% CGO – 40 mol.% GSFT green pellets sintered on  $\text{Al}_2\text{O}_3$  substrates at  $1450\text{ }^\circ\text{C}$  in ambient air for 5, 10 and 20 hours. The scale bar is  $10\text{ }\mu\text{m}$ .

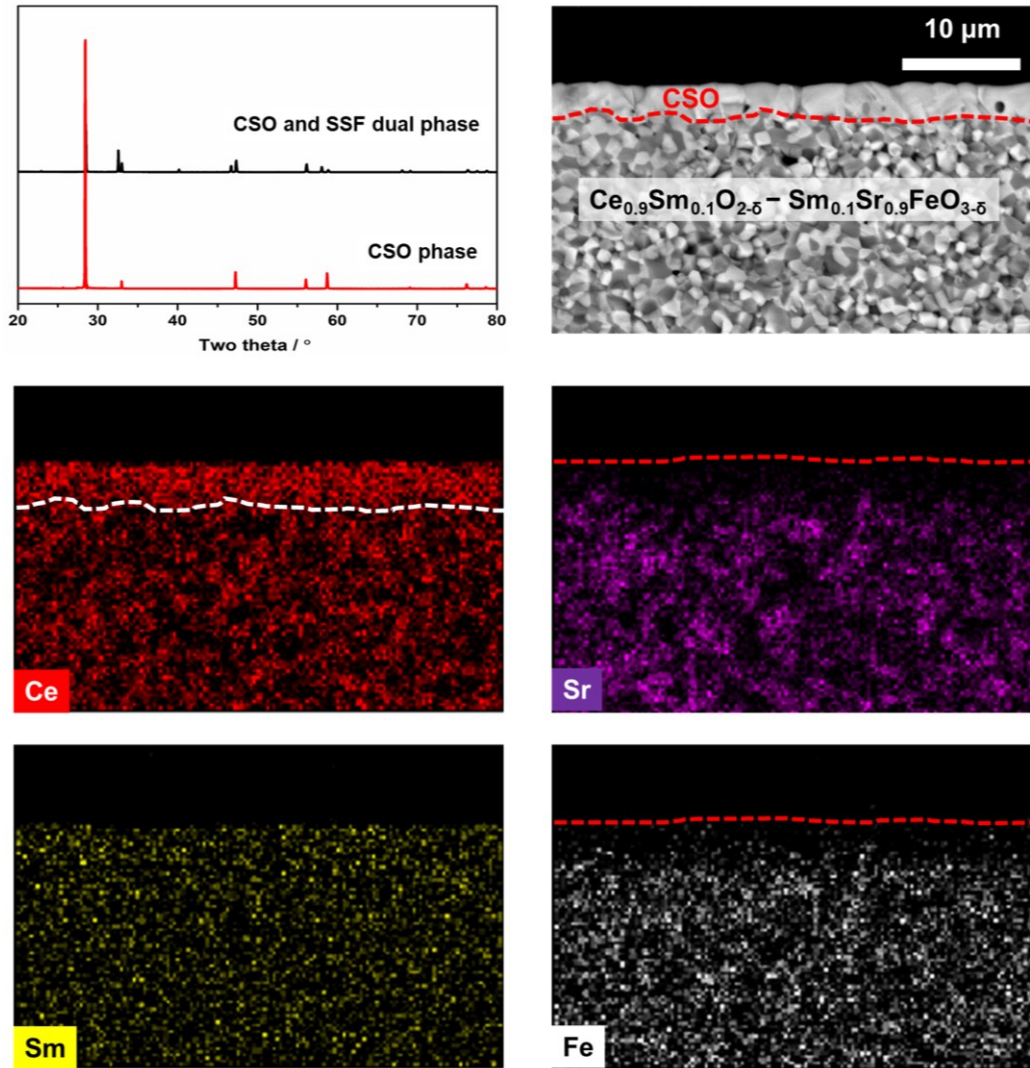
The thickness of the CGO layer increases with increasing sintering dwell time from 5 to 20 hours at  $1450\text{ }^\circ\text{C}$  (Fig. S6), indicating that interface-reaction-induced CGO rearrangement is relevant for the dwell time. We note that sintering conditions for the multilayered ceramic membrane with CGO thin layers may not be optimized and, in the future, optimum conditions will be determined to obtain better membrane performance.



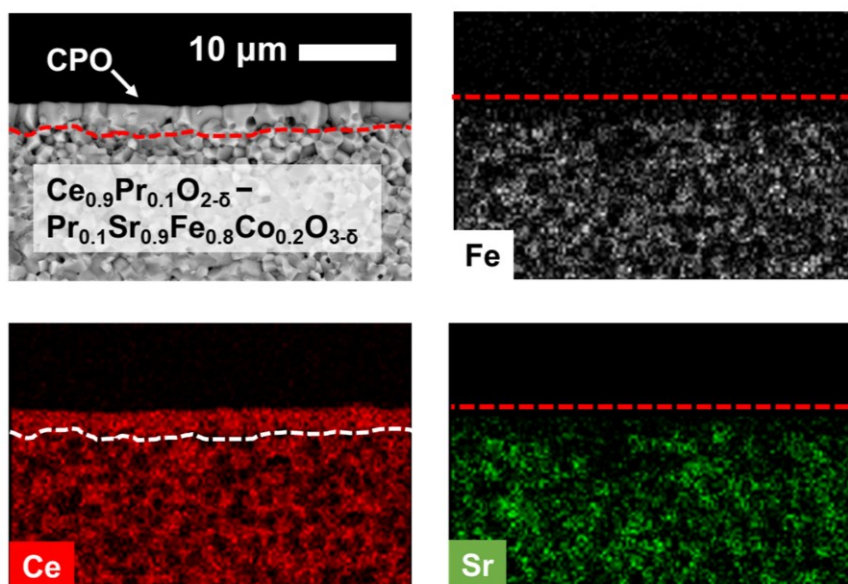
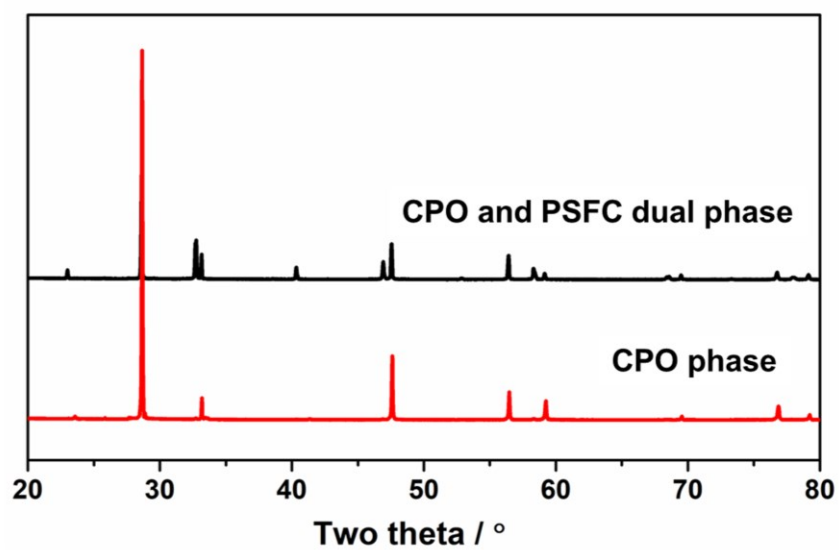
**Figure S7.**

BSE analyses of cross-sections of CGO-GSFT green pellets with molar ratios of 30/70, 60/40 and 70/30 sintered on  $\text{Al}_2\text{O}_3$  substrates at 1450 °C in ambient air for 10 hours.

As shown in Fig. S7, the thickness of the CGO layer increases with increasing CGO/CGFT ratio in the precursor binary oxides from 30/70, 60/40 and 70/30, indicating that interface-reaction-induced CGO rearrangement is relevant for the surface composition.

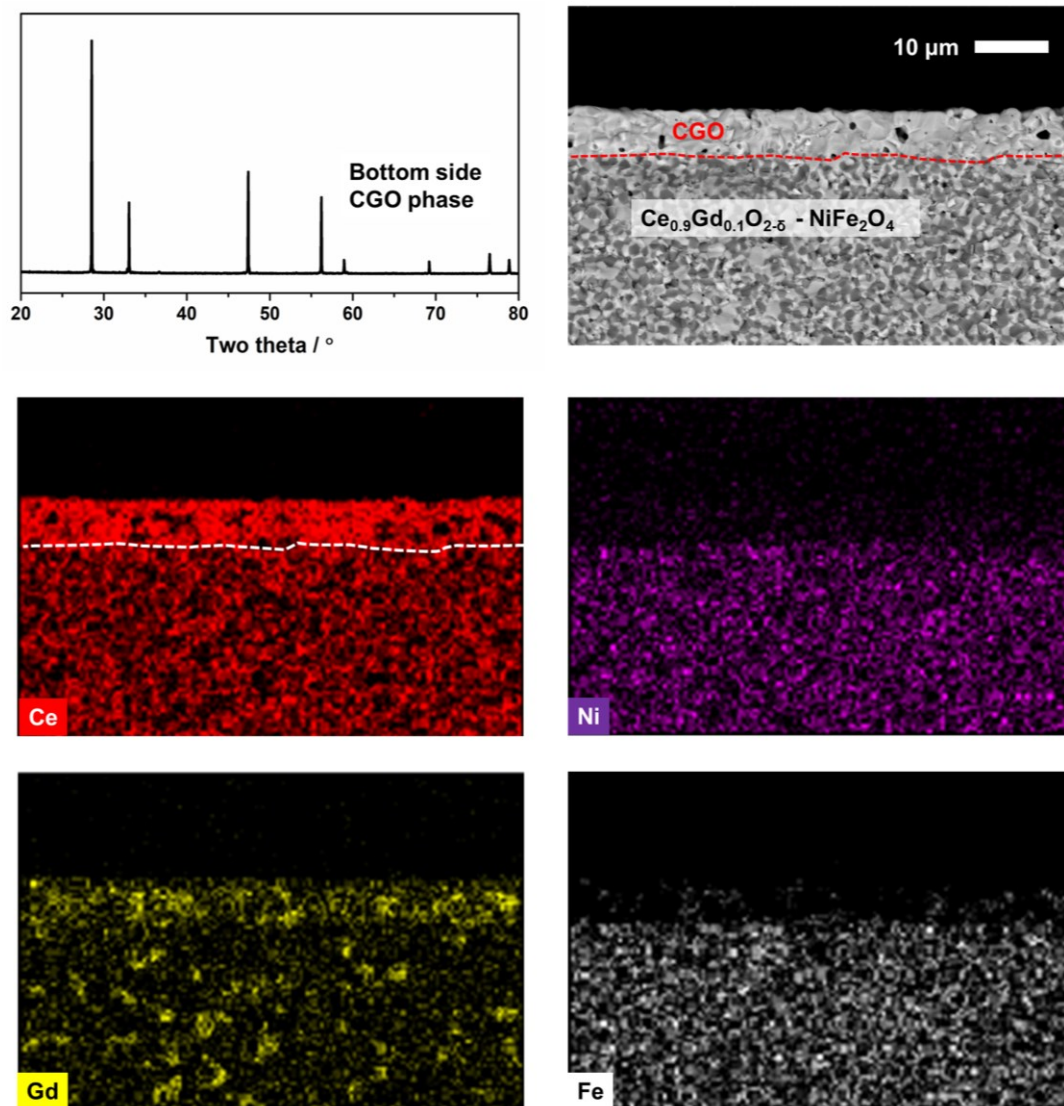


**Figure S8.** XRD and BSE-EDX analyses of a CSO/(CSO-SSF) layered ceramic membrane after a single sintering process.

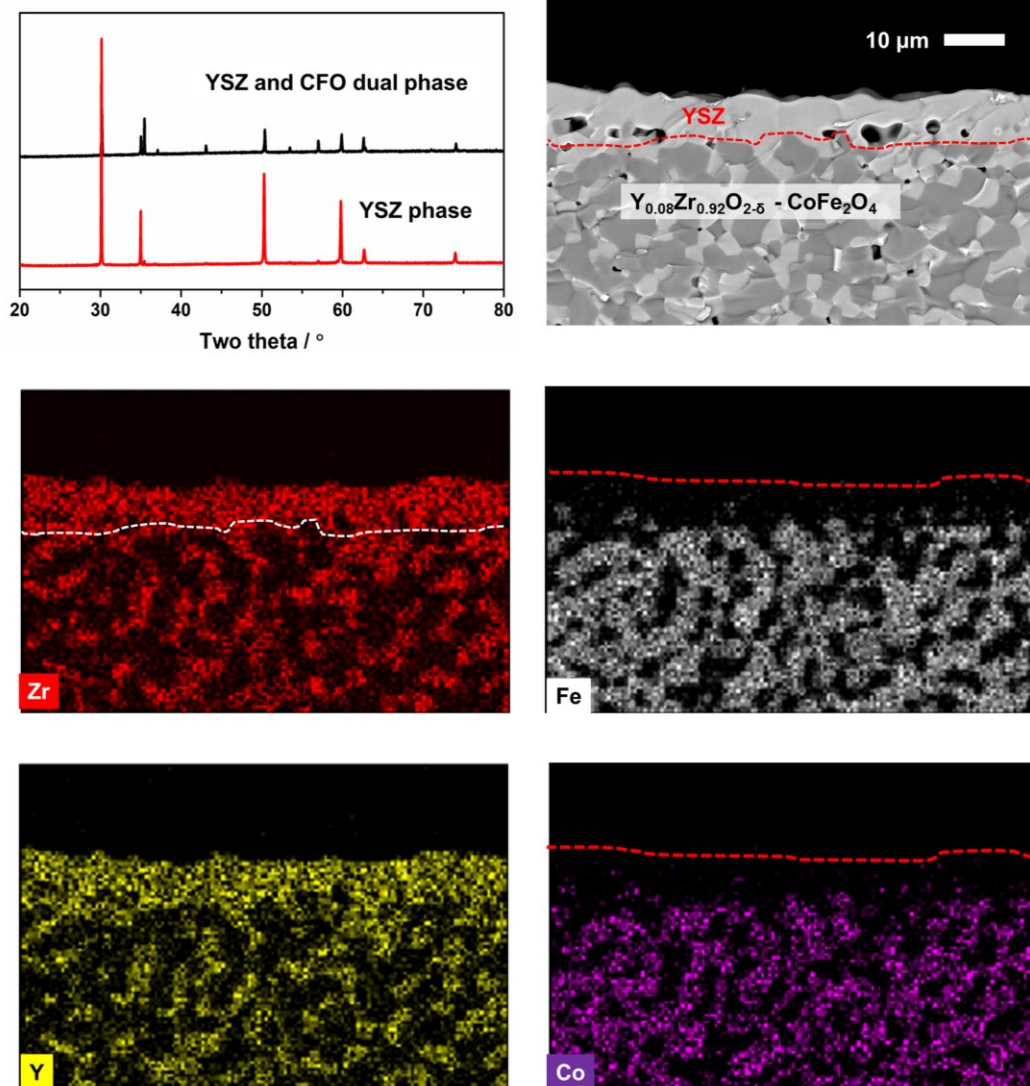


**Figure S9.**

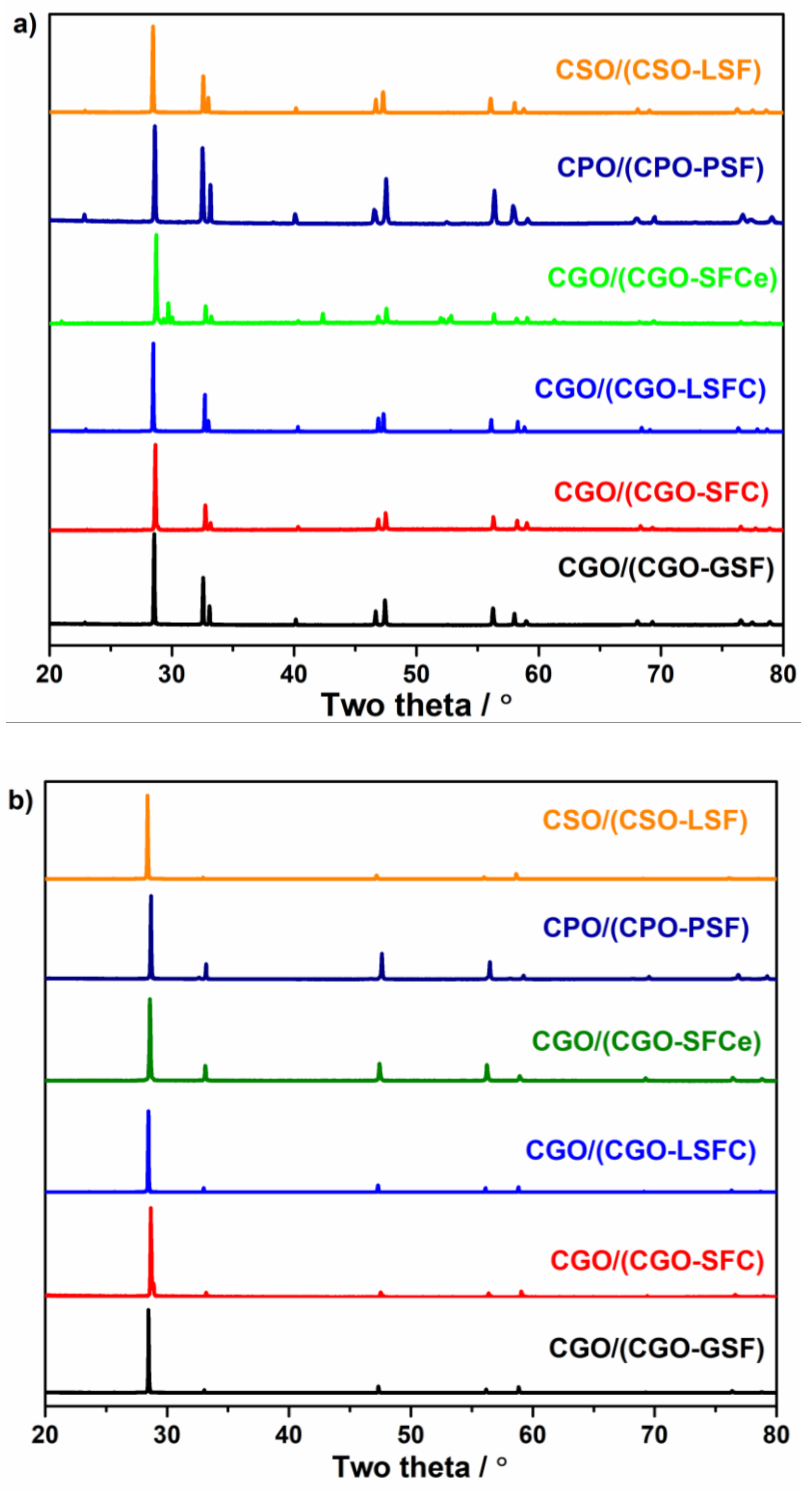
XRD and BSE-EDX analyses of a CPO/(CPO-PSFC) layered ceramic membrane after a single sintering process.



**Figure S10.**  
XRD and BSE-EDX analyses of a CGO/(CGO-NFO) layered ceramic membrane after a single sintering process.

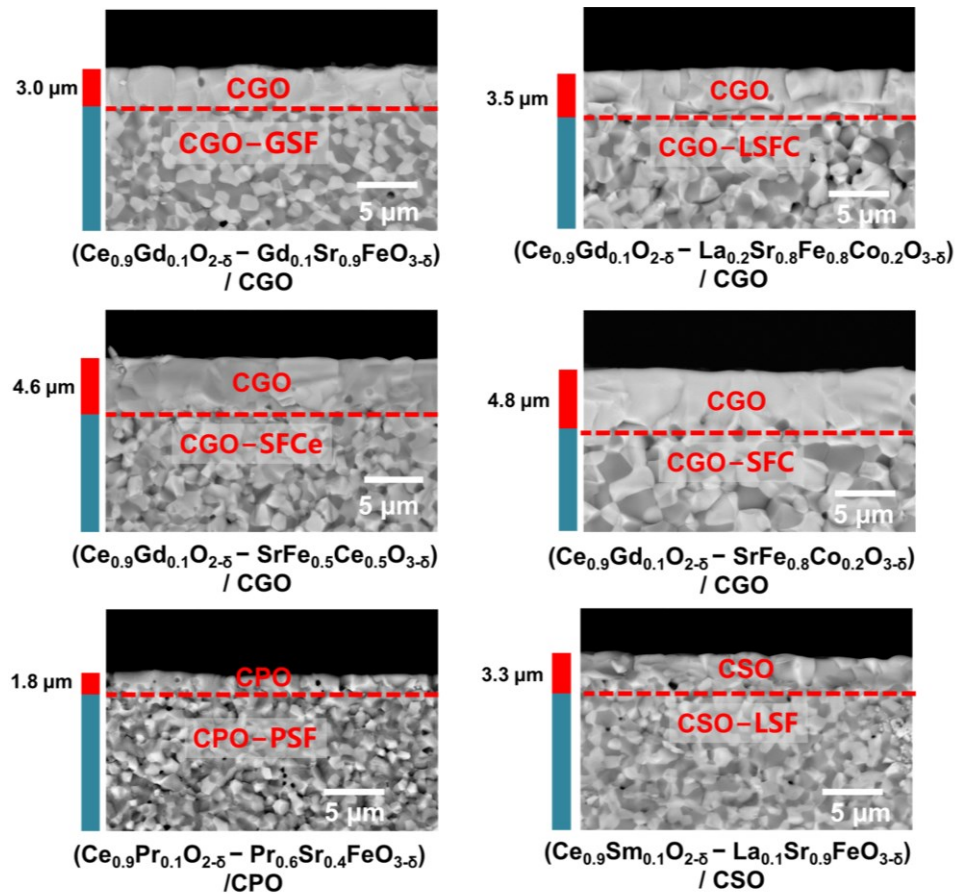


**Figure S11.**  
 XRD and BSE-EDX analyses of a YSZ/(YSZ-CFO) layered ceramic membrane after a single sintering process.



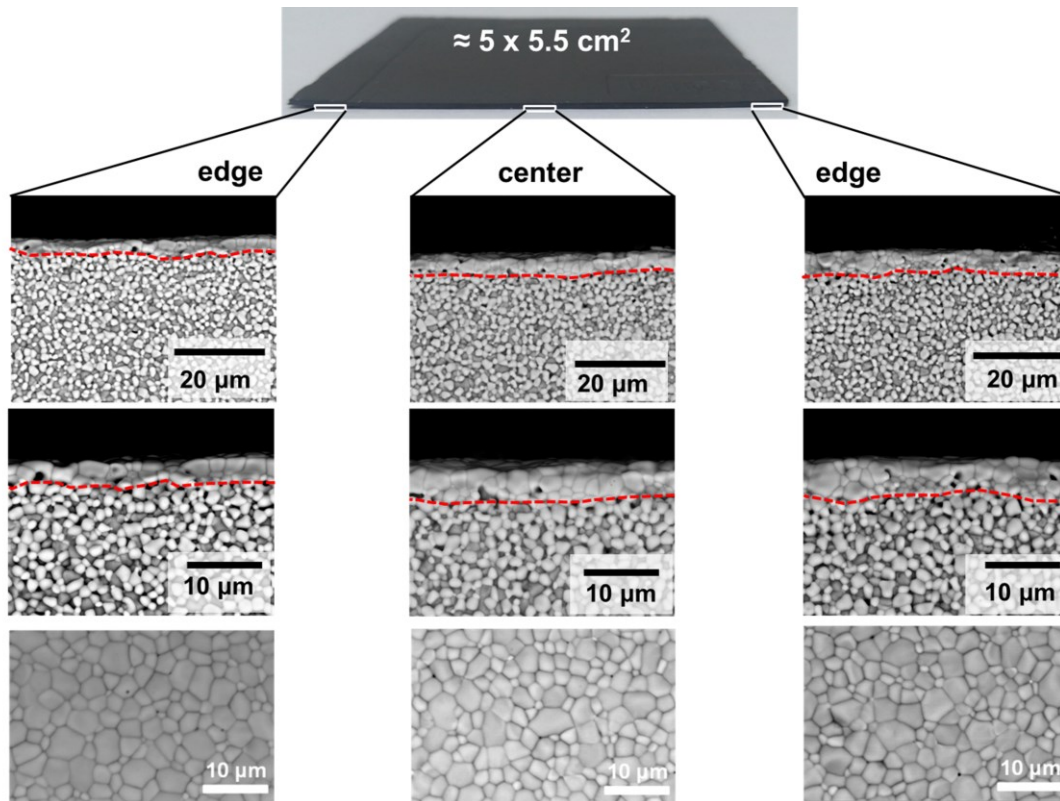
**Figure S12.**

XRD analysis of (a) dual-phase and (b) ceria phase (b) surfaces of the other six CeO<sub>2</sub> – SrFeO<sub>3</sub> composites sintered on Al<sub>2</sub>O<sub>3</sub> substrates after one single sintering process.



**Figure S13.**

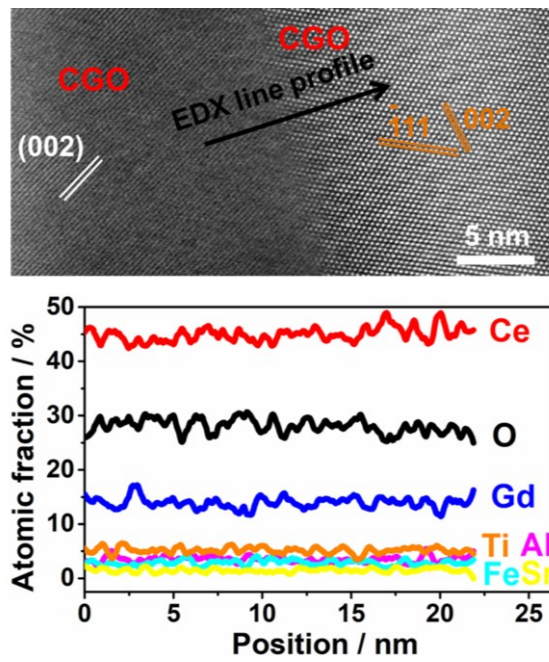
BSE analyses of cross-sections of the other six  $\text{CeO}_2 - \text{SrFeO}_3$  composites sintered on  $\text{Al}_2\text{O}_3$  substrates after one single sintering process.



**Figure S14.**

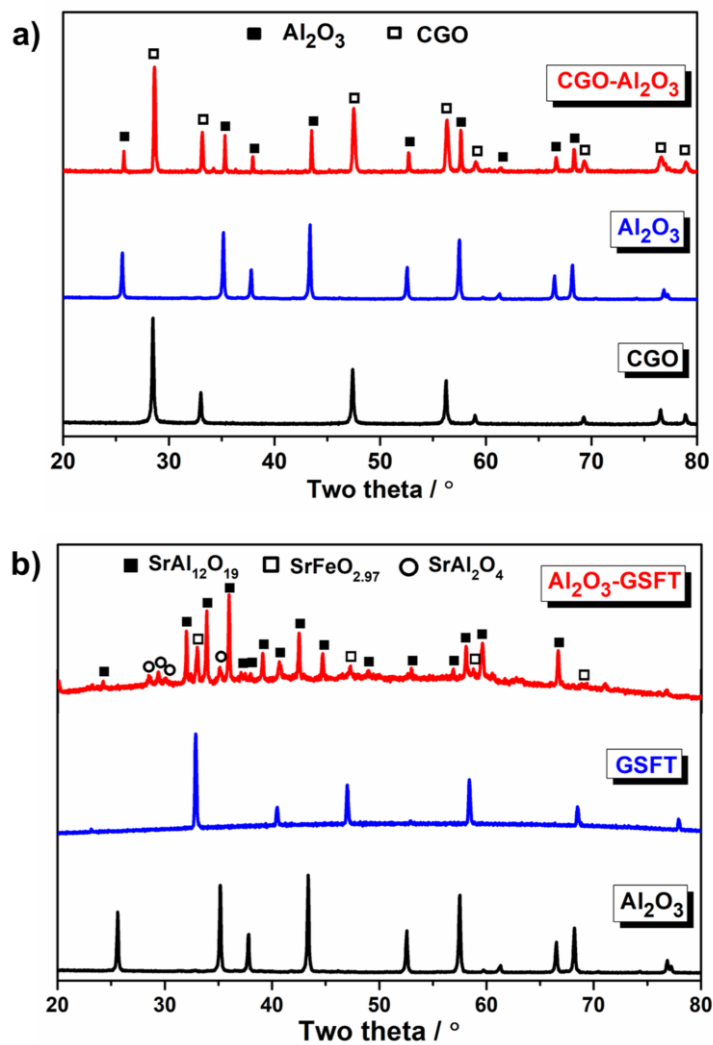
BSE images of an approximately  $5 \times 5.5 \text{ cm}^2$  CGO/(CGO-GSFT) layered ceramic sample, in which the CGO layer was flat, thin ( $\sim 2 \mu\text{m}$ ) and completely dense.

Figure S14 shows the morphology and phase composition of an approximately  $5 \times 5.5 \text{ cm}^2$  flat sample, in which the CGO layer was thin ( $\sim 2 \mu\text{m}$ ), dense and well-adhered to the support layer, indicating that the approach also enables the scalable fabrication of large-area, flat multilayer sheets with CGO conducting thin layers.



**Figure S15.**

Elemental composition analysis: EDX line profiles recorded across an interface between two CGO grains from the region marked by a black arrow in the upper HAADF STEM image.



**Figure S16.**

XRD analysis of (a) CGO-Al<sub>2</sub>O<sub>3</sub> and (b) GSFT-Al<sub>2</sub>O<sub>3</sub> powders co-fired in ambient air for 10 hours at 1450 and 1350 °C, respectively.

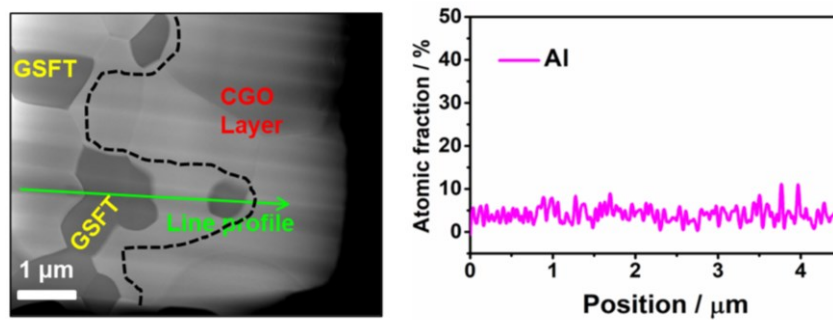


**Figure S17.**

EDX elemental profile of Al recorded from the intermediate layer to the CGO dense layer, as marked by a green arrow in the HAADF STEM image, showing that the Al concentration is low and homogenous in both layers to within the detection limit of the measurement.

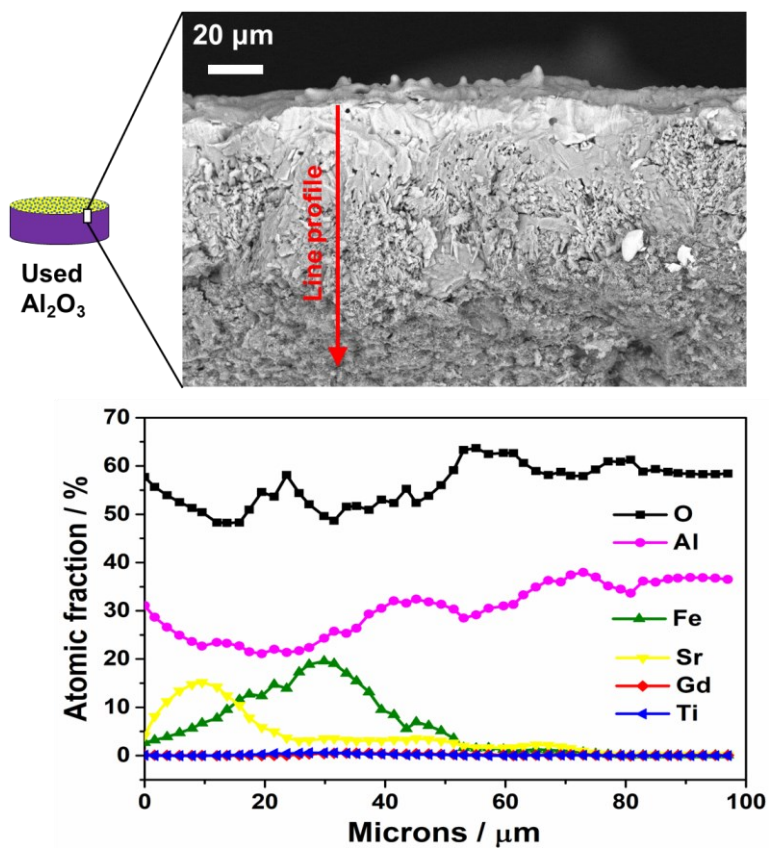


**Figure S18.**

EDX line scan profiles of the cross-sectional interface of the spent Al<sub>2</sub>O<sub>3</sub> after sintering a GSFT disk on an Al<sub>2</sub>O<sub>3</sub> substrate at 1400 °C for 5h.

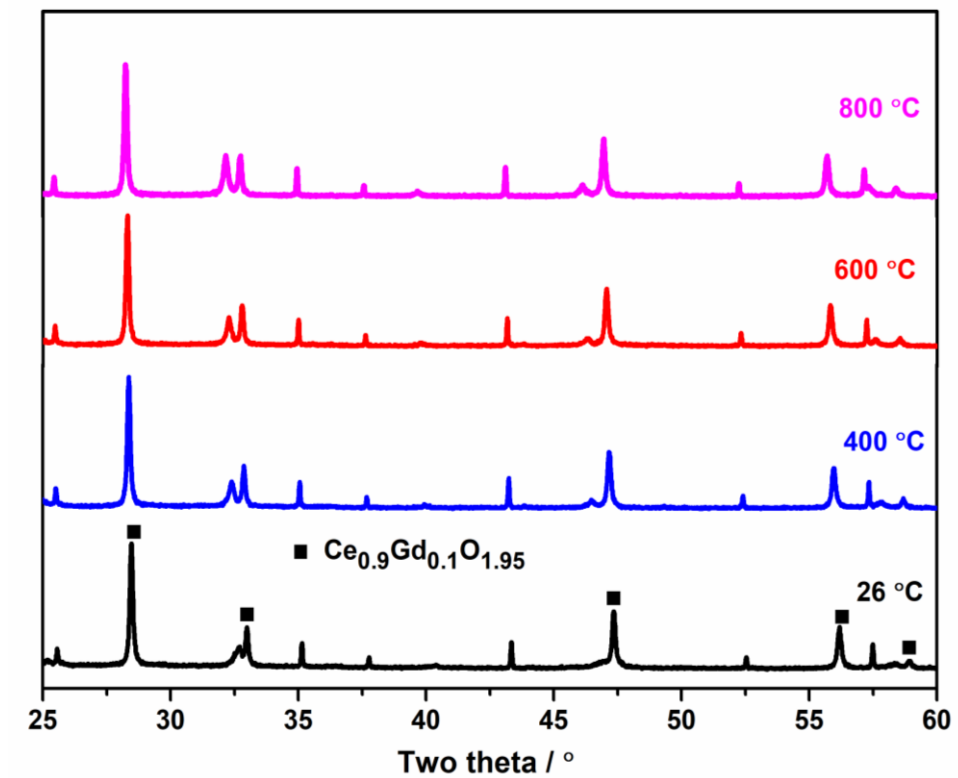


**Figure S19.**

*In situ* X-ray diffraction of CGO-GSFT-Al<sub>2</sub>O<sub>3</sub> composite powders recorded during heating from room temperature to 800 °C in ambient atmosphere.

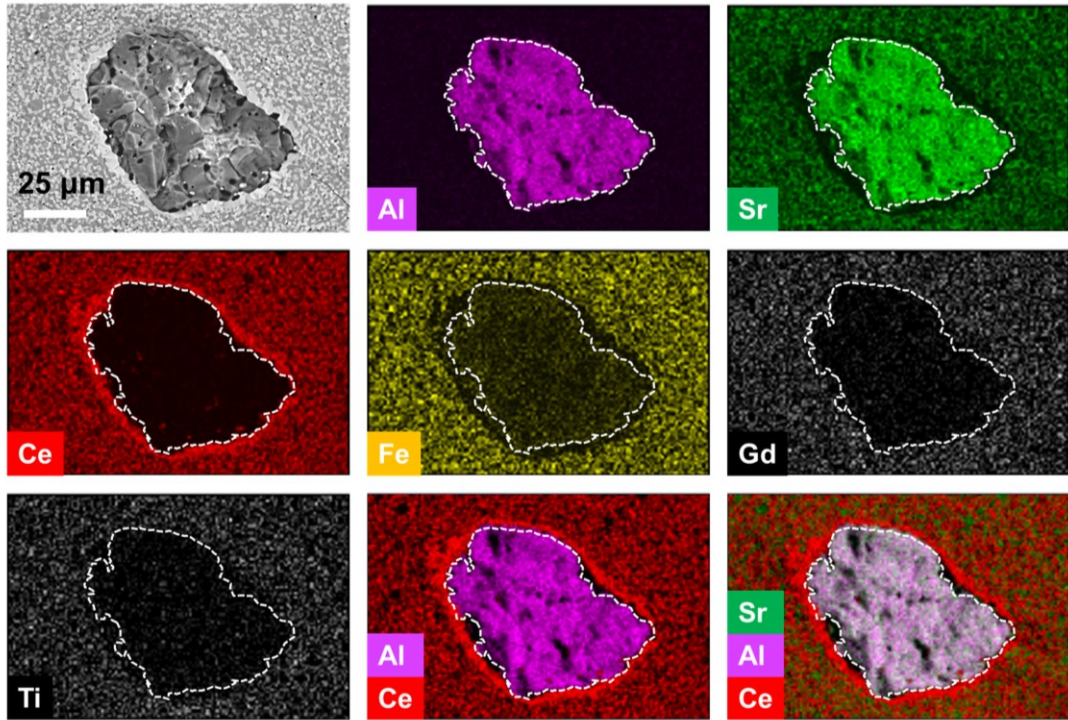


**Figure S20.**

BSE image and EDX elemental maps of Al, Ce, Sr, Fe, Gd and Ti around an  $\text{Al}_2\text{O}_3$  particle in a CGO-GSFT disk after sintering at 1450 °C.

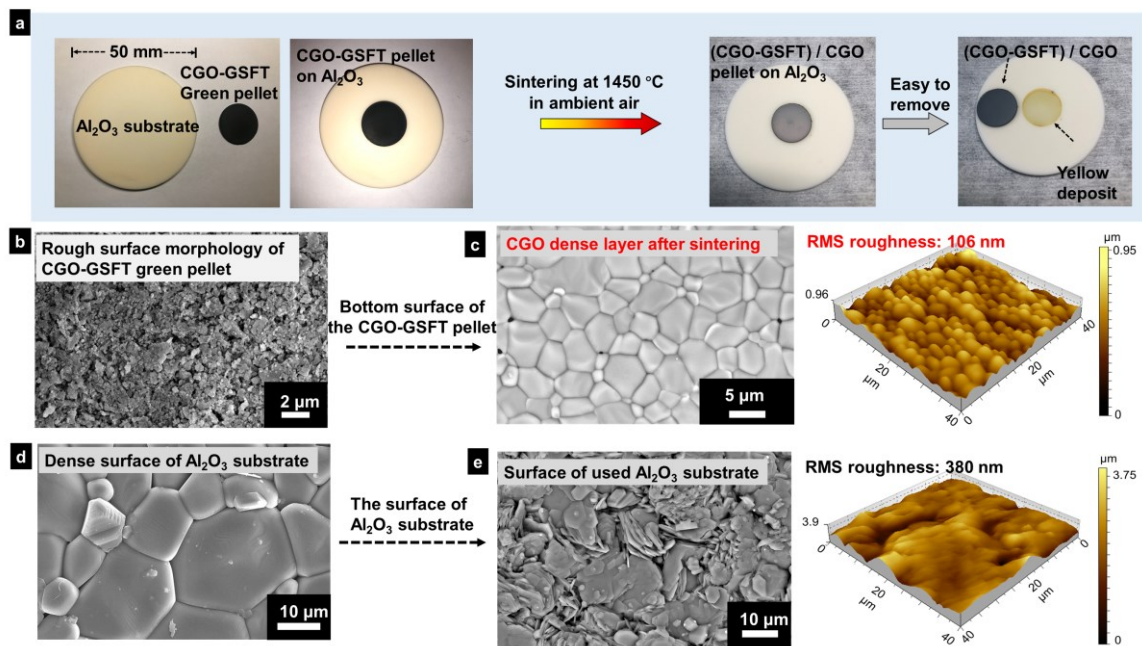


**Figure S21.**

The surface morphology of the CGO-GSFT membrane and the  $\text{Al}_2\text{O}_3$  substrate before and after sintering at  $1450\text{ }^\circ\text{C}$  in ambient air. (a) The fabrication procedure of bi-layered (CGO-GSFT) / CGO membrane; (b) SEM image of the surface of pressed CGO-GSFT green pellet; (c) SEM and AFM images of the CGO layer of the (CGO-GSFT) / CGO membrane; (d) SEM image of the surface of the fresh  $\text{Al}_2\text{O}_3$  substrate; (e) SEM and AFM images of the yellow deposit on the spent  $\text{Al}_2\text{O}_3$  substrate.

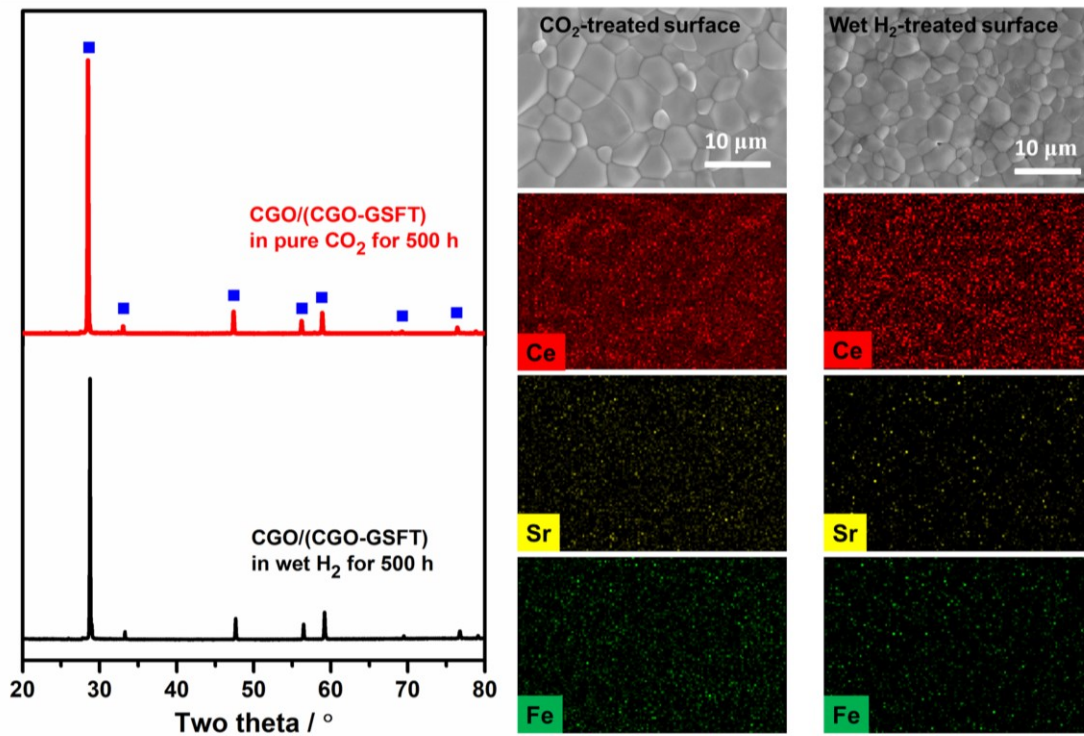


**Figure S22.**

XRD analyses and EDX maps of the CGO layer in a CGO/(CGO-GSFT) layered ceramic membrane after treatment at 750 °C in pure CO<sub>2</sub> and 3 vol.% H<sub>2</sub>O - 97 vol.% H<sub>2</sub> atmospheres for 500 hours.

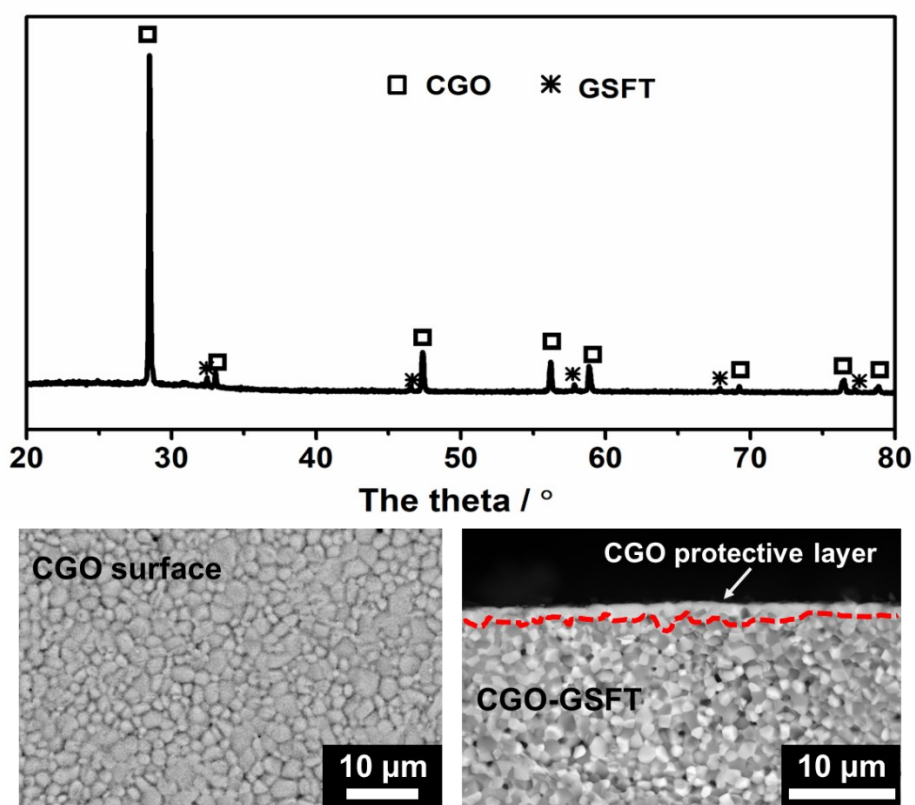


**Figure S23.**

XRD analysis and BSE images of the CGO layer in a CGO/(CGO-GSFT) layered ceramic membrane after the long-term test.

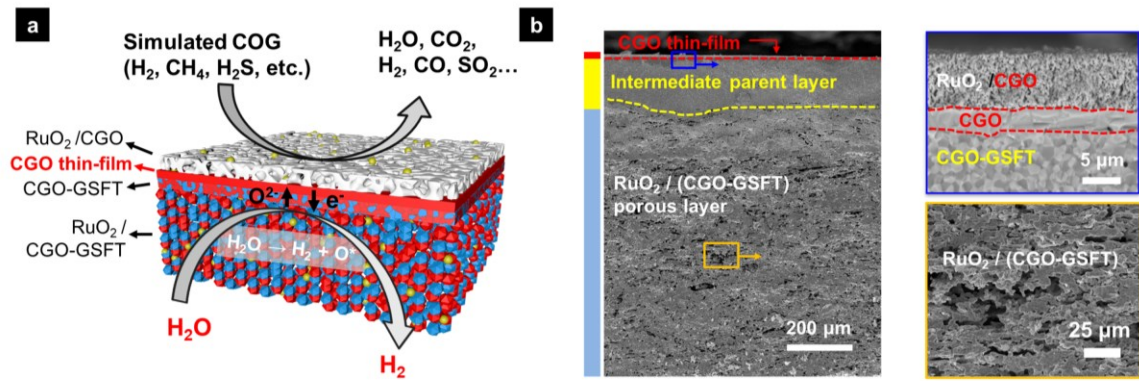


**Figure S24**

(a) Schematic diagram of a CGO/(CGO-GSFT)/porous (CGO-GSFT) three-layered membrane reactor. (b) SEM/BSE images of the three-layered membrane coated with a RuO<sub>2</sub>@CGO porous layer.

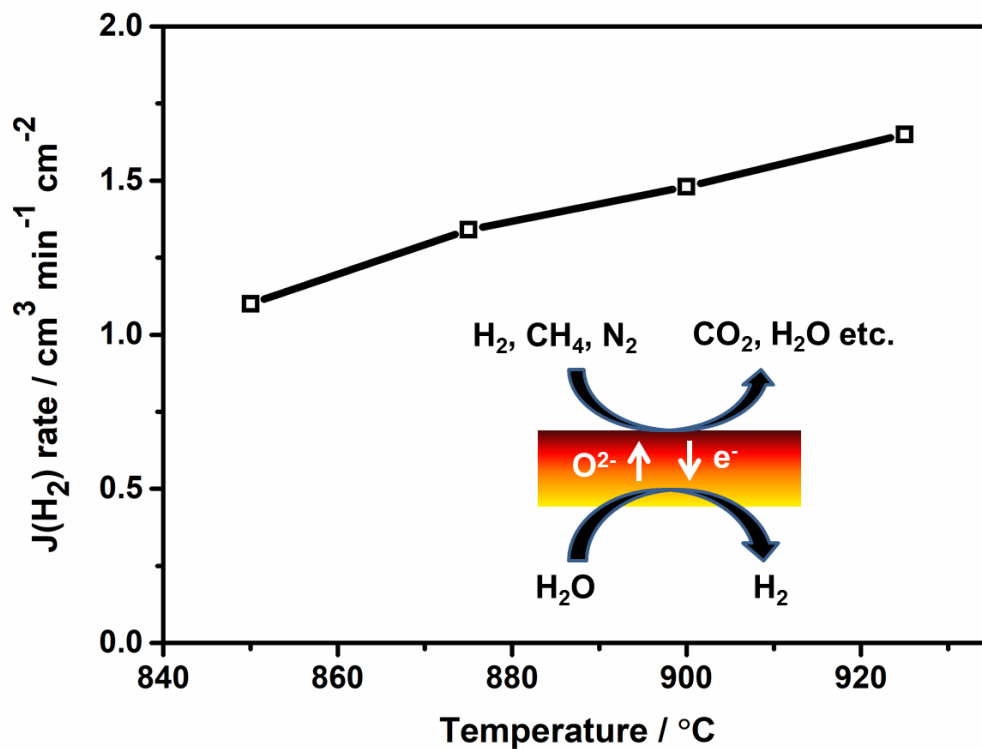


**Figure S25.**

Effect of operating temperature on hydrogen production rate from water splitting driven by simulated COG conversion in a CGO/(CGO-GSFT)/p(CGO-GSFT) multilayered membrane reactor. H<sub>2</sub>O side: H<sub>2</sub>O/He = 20/5 cm<sup>3</sup> min<sup>-1</sup>; simulated COG side: H<sub>2</sub>/CH<sub>4</sub>/N<sub>2</sub> = 2.5/0.5/3 cm<sup>3</sup> min<sup>-1</sup>.

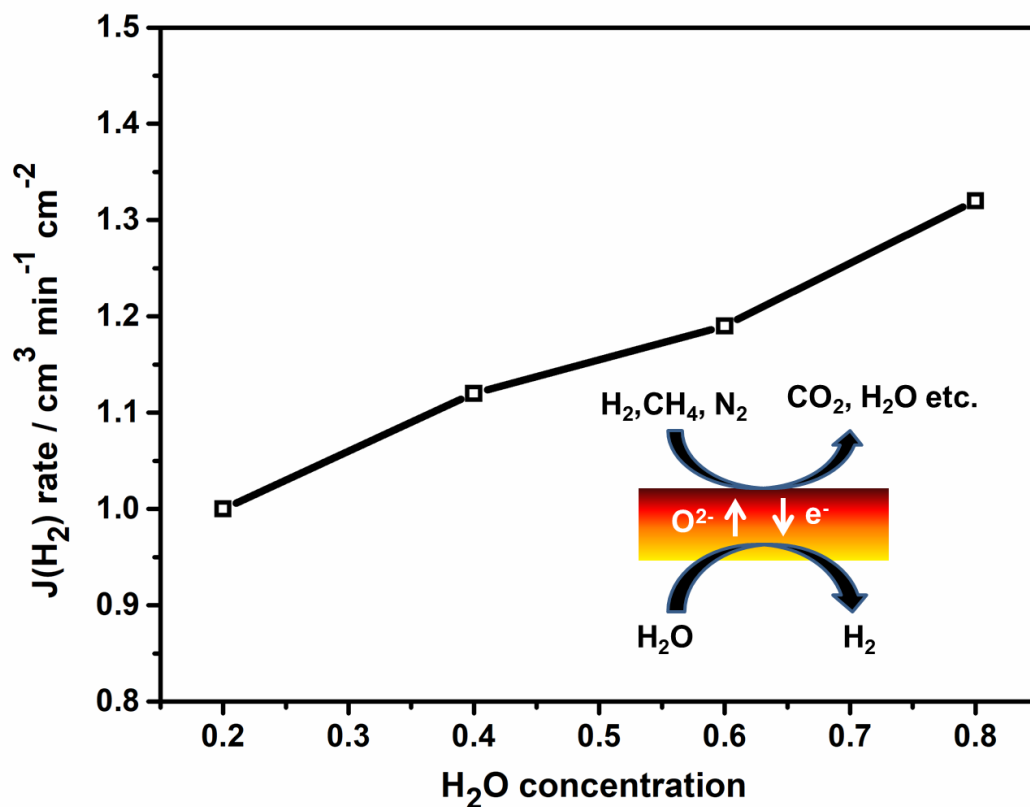


**Figure S26.**

Effect of H<sub>2</sub>O concentration on the steam side on hydrogen production rate from water splitting driven by simulated COG conversion in a CGO/(CGO-GSFT)/p(CGO-GSFT) multilayered membrane reactor. H<sub>2</sub>O side:  $F(\text{total})=25 \text{ cm}^3 \text{ min}^{-1}$  with H<sub>2</sub>O concentrations of 20, 40, 60 and 80 vol.%; simulated COG side: H<sub>2</sub>/CH<sub>4</sub>/N<sub>2</sub> = 2.5/0.5/3 cm<sup>3</sup> min<sup>-1</sup>. Temperature: 925 °C.

**Table S1:** Ten different bilayer ceramic membranes with dense thin layers of  $\text{Ce}_{1-x}\text{M}_x\text{O}_{2-\delta}$  (M= Gd, Sm, Pr) or  $\text{Y}_{0.08}\text{Zr}_{0.92}\text{O}_{2-\delta}$  (YSZ) fabricated by single-step sintering.

Starting dual phase precursors		Ion conducting dense thin layer	Sintering temperature
$\text{Ce}_{0.9}\text{Sm}_{0.1}\text{O}_{2-\delta}$ (CSO)	$\text{Sm}_{0.1}\text{Sr}_{0.9}\text{FeO}_{3-\delta}$ (SSF)	CSO	1400 °C
$\text{Ce}_{0.9}\text{Pr}_{0.1}\text{O}_{2-\delta}$ (CPO)	$\text{Pr}_{0.1}\text{Sr}_{0.9}\text{Fe}_{0.8}\text{Co}_{0.2}\text{O}_{3-\delta}$ (PSFC)	CPO	1400 °C
$\text{Ce}_{0.9}\text{Gd}_{0.1}\text{O}_{2-\delta}$ (CGO)	$\text{NiFe}_2\text{O}_4$ (NFO)	CGO	1400 °C
$\text{Y}_{0.08}\text{Zr}_{0.92}\text{O}_{2-\delta}$ (YSZ)	$\text{CoFe}_2\text{O}_4$ (CFO)	YSZ	1450 °C
$\text{Ce}_{0.9}\text{Gd}_{0.1}\text{O}_{2-\delta}$ (CGO)	$\text{Gd}_{0.1}\text{Sr}_{0.9}\text{FeO}_{3-\delta}$ (GSF)	CGO	1400 °C
$\text{Ce}_{0.9}\text{Gd}_{0.1}\text{O}_{2-\delta}$ (CGO)	$\text{SrFe}_{0.8}\text{Co}_{0.2}\text{O}_{3-\delta}$ (SFC)	CGO	1400 °C
$\text{Ce}_{0.9}\text{Gd}_{0.1}\text{O}_{2-\delta}$ (CGO)	$\text{La}_{0.2}\text{Sr}_{0.8}\text{Fe}_{0.8}\text{Co}_{0.2}\text{O}_{3-\delta}$ (LSFC)	CGO	1400 °C
$\text{Ce}_{0.9}\text{Gd}_{0.1}\text{O}_{2-\delta}$ (CGO)	$\text{SrFe}_{0.5}\text{Ce}_{0.5}\text{O}_{3-\delta}$ (SFCE)	CGO	1380 °C
$\text{Ce}_{0.9}\text{Pr}_{0.1}\text{O}_{2-\delta}$ (CPO)	$\text{Pr}_{0.6}\text{Sr}_{0.4}\text{FeO}_{3-\delta}$ (PSF)	CPO	1400 °C
$\text{Ce}_{0.9}\text{Sm}_{0.1}\text{O}_{2-\delta}$ (CSO)	$\text{La}_{0.1}\text{Sr}_{0.9}\text{FeO}_{3-\delta}$ (LSF)	CSO	1400 °C

## References

- [1] G. He, T. Hu, H. Zhou, F. Liang, S. Baumann, W. A. Meulenbergh, H. Jiang, *Ind. Eng. Chem. Res.* **2017**, *56*, 10134-10141.
- [2] G. He, W. Liang, C.-L. Tsai, X. Xia, S. Baumann, H. Jiang, W. A. Meulenbergh, *iScience* **2019**, *19*, 955-964.
- [3] W. Liang, Z. Cao, G. He, J. Caro, H. Jiang, *ACS Sustain. Chem. Eng.* **2017**, *5*, 8657-8662.
- [4] W. Fang, F. Steinbach, Z. Cao, X. Zhu, A. Feldhoff, *Angew. Chem. Int. Ed.* **2016**, *128*, 8790-8793.
- [5] C. W. Bale, E. Bélisle, P. Chartrand, S. A. Decterov, G. Eriksson, A. E. Gheribi, K. Hack, I. H. Jung, Y. B. Kang, J. Melançon, A. D. Pelton, S. Petersen, C. Robelin, J. Sangster, P. Spencer, M. A. Van Ende, *Calphad* **2016**, *54*, 35-53.
- [6] a) The ab initio materials project (AIMP) compound database, GTT-Technologies; b) The Materials Project ([www.materialsproject.org](http://www.materialsproject.org)).
- [7] a) O. H. Krikorian, *High Temp. - High Pressures* **1988**, *20*: 2; b) S. I. D. A. Ditmars, S. S. Chang, G. Bernstein, *J. Res. National Bureau Stand.* **1982**, *87*, 159-163; c) O. K. I. Barin, *Thermochemical Properties of Inorganic Substances*, Springer-Verlag Berlin, Duesseldorf, **1973**.
- [8] P. Kamakoti, B. D. Morreale, M. V. Ciocco, B. H. Howard, R. P. Killmeyer, A. V. Cugini, D. S. Sholl, *Science* **2005**, *307*, 569-573.
- [9] H. J. Moon, S. Baumann, S. Uhlenbruck, D. Sebold, W. A. Meulenbergh, H. Park, *Thin Solid Films* **2012**, *526*, 59-64.
- [10] S. Cheng, C. Chatzichristodoulou, M. Søggaard, A. Kaiser, P. V. Hendriksen, *J. Electrochem. Soc.* **2017**, *164*, F1354-F1367.
- [11] L. Jia, G. He, Y. Zhang, J. Caro, H. Jiang, *Angew. Chem. Int. Ed.* **2021**, *60*, 5204-5208.